ADVANCED FUNCTIONAL MATERIALS

FULL PAPER

DOI: 10.1002/adfm.200600458

Highly Dispersed Mixed Zirconia and Hafnia Nanoparticles in a Silica Matrix: First Example of a ZrO_2–HfO_2–SiO_2 Ternary Oxide System**

By *Lidia Armelao*, *Helmut Bertagnolli*, *Davide Bleiner*, *Matthijs Groenewolt*, *Silvia Gross*,* *Venkata Krishnan*, *Cinzia Sada*, *Ulrich Schubert*, *Eugenio Tondello*, and *Andrea Zattin*

ZrO_2 and HfO_2 nanoparticles are homogeneously dispersed in SiO_2 matrices (supported film and bulk powders) by copolymerization of two oxozirconium and oxohafnium clusters ($M_4O_2(OMc)_{12}$, M = Zr, Hf; OMc = OC(O)–C(CH_3)=CH_2) with (methacryloxypropyl)trimethoxysilane (MAPTMS, (CH2=C(CH_3)C(O)O)–(CH_2)$_3$Si(OCH_3)$_3$). After calcination (at a temperature ≥800 °C), a silica matrix with homogeneously distributed MO_2 nanocrystallites is obtained. This route yields a spatially homogeneous dispersion of the metal precursors inside the silica matrix, which is maintained during calcination. The composition of the films and the powders is studied before and after calcination by using Fourier transform infrared (FTIR) analysis, X-ray photoelectron spectroscopy (XPS), secondary ion mass spectrometry (SIMS), and laser ablation inductively coupled plasma mass spectrometry (LA-ICPMS). The local environment of the metal atoms in one of the calcined samples is investigated by using X-ray Absorption Fine Structure (XAFS) spectroscopy. Through X-ray diffraction (XRD) the crystallization of Hf and Zr oxides is seen at temperatures higher than those expected for the pure oxides, and transmission electron microscopy (TEM) shows the presence of well-distributed and isolated crystalline oxide nanoparticles (5–10 nm).

[*] Dr. S. Gross, Dr. L. Armelao, Prof. E. Tondello, A. Zattin
CNR-ISTM, Department of Chemistry
University of Padova and INSTM
via Marzolo, 1, 35131 Padova (Italy)
E-mail: silvia.gross@unipd.it
Prof. H. Bertagnolli, Dr. V. Krishnan
Institut für Physikalische Chemie, Universität Stuttgart
Pfaffenwaldring 55, 70569 Stuttgart (Germany)
Dr. D. Bleiner
Department of Chemistry, University of Antwerp
Universiteitsplein 1, 2610 Wilrijk-Antwerp (Belgium)
Dr. M. Groenewolt[+]
Max-Planck-Institut für Kolloid- und Grenzflächenforschung
Am Mühlenberg 1, 14476 Potsdam, Golm (Germany)
Dr. C. Sada
Dipartimento di Fisica, Università degli Studi di Padova
Via Marzolo, 8, 35131 Padova (Italy)
Prof. U. Schubert
Institut für Materialchemie, Technische Universität Wien
Getreidemarkt 9/2/7 1060 Vienna (Austria)
[+] Present address: BASF-Coatings AG, Glasuritstraße, 1, 48136 Münster, Germany.

[**] The National Research Council (CNR), Italy, the research program INSTM-PRISMA "High-k oxide-based thin films from liquid and vapor phase routes", and the Fonds zur Förderung der wissenschaftlichen Forschung (FWF), Austria, are acknowledged for financial support. Italian Rectors Conference (CRUI), Ministero degli Affari Esteri, Rome, Italy, Österreichischer Austausch dienst (ÖAD), Vienna, Austria are gratefully acknowledged for the funding of the researchers mobility in the framework of the Italy–Germany and Italy–Austria bilateral programs. We thank HASYLAB at DESY, Hamburg for the provision of synchrotron radiation for EXAFS measurements. S. Gross gratefully thanks the Deutscher Akademischer Austauschdienst (DAAD), Bonn (Germany), for the awarding of a DAAD grant to finance a research period in Germany. Ciba Specialty Chemicals, Basel, Switzerland, is acknowledged for the kind supply of Irgacure 184. The EMPA laboratories are acknowledged for LA-ICPMS infrastructure.

1. Introduction

Zirconium (zirconia, ZrO_2) and hafnium (hafnia, HfO_2) dioxides are ceramic materials characterized by high thermal and chemical stability, high dielectric constant, improved mechanical strength, catalytic properties, and low electrical conductivity.[1,2] Embedding these oxides in silica can lead to a noticeable enhancement of the properties of SiO_2, at the same time allowing to overcome problems related to the use of pure Zr and Hf dioxides, such as high cost and low specific surface area. Zirconia–silica glasses have been proposed as structural materials thanks to their low thermal expansion, high toughness, and excellent resistance to chemicals.[1,2] Furthermore, both binary ZrO_2–SiO_2 and HfO_2–SiO_2 systems are appealing materials for the development of high-κ films to overcome limitations in the fabrication of integrated circuits.[3–7] The embedding of guest particles in a transparent and dielectric matrix enables fine tailoring of its optical properties,[8] such as refractive index. In the form of powder these mixed oxides are also attracting a growing interest both as catalysts[9–13] as well as catalyst supports.[14]

The obtainment of host particles even dispersion in the guest matrix is a requirement to be met in order to get the desired properties. As a consequence, since the properties of these binary systems are strongly affected by the composition, the microstructure, and the degree of mixing of the different oxide components, suitable synthetic routes ensuring the achievement of the required purity and homogeneity have to be found. Reported approaches to these binary systems include chemical solution deposition,[15] ultrahigh vacuum molecular beam epi-

taxy,[7] and conventional sol–gel processing starting from the corresponding alkoxides.[16–27]

With respect to the above-mentioned approaches, our route based on the copolymerisation of a Zr and Hf cluster with a methacryloxytriethoxysilane enables the preparation of nanostructured binary oxides characterized by homogeneity at a molecular level. A similar strategy has been pioneered by Schubert and co-workers,[28–30] who have developed a siloxane-derived precursor bearing a β-diketonate moiety which can coordinate transition metals, for instance titanium, thus affording a hybrid single-source precursor for silica–titania mixed-oxide materials.

In recent years, Mountjoy and co-workers[26,31] have developed ternary oxide systems based on TiO_2–ZrO_2–SiO_2, while Mao et al.[32] have described a different synthesis route to ternary metal-oxide nanostructures. In all these studies, the preparation of the mixed oxides was addressed using a conventional sol–gel process starting from the corresponding metal alkoxides. To the best of our knowledge, no ternary system of the type $(Hf,Zr)O_2$:SiO_2 has been prepared up to now. In this study, inorganic–organic hybrid materials with the metal-oxide precursors homogenously embedded in a silica matrix were used as "composite precursors" for the preparation of binary oxide systems of the type MO_x:SiO_2 with the metal oxide homogeneously dispersed in the silica matrix. Calcination of the starting hybrid materials at high temperature (> 800 °C) promotes pyrolysis of the organic parts and densification of the oxide networks, thus enabling the preparation of pure and homogeneous nanostructured oxide materials, both as powders and films. In the present work, we extended an already optimized synthetic procedure, which has been used to prepare ZrO_2–SiO_2 and HfO_2–SiO_2 nanostructure-based materials,[33–38] to the preparation of silica-based materials embedding both zirconia and hafnia nanoparticles. The method relies on the use of methacrylate-substituted transition-metal oxoclusters $M_4O_2(OMc)_{12}$ and methacryloxypropyltrimethoxysilane as molecular building blocks. These clusters are synthesized by the reaction of metal alkoxides with methacrylic acid, as reported elsewhere.[39,40] The methacrylate moieties of the cluster and that of the silane are copolymerized, while the alkoxy groups of the silane undergo hydrolysis and condensation reactions to form a silica network. These and similar metal oxoclusters have been already used as inorganic building blocks for the synthesis of a wide variety of inorganic–organic hybrid materials.[41–44]

After preparation, the oxides were analyzed. In particular, the composition, morphology, and microstructure of ZrO_2–HfO_2–SiO_2 (Si/(Zr+Hf) = 10, 20, 40 molar ratio) films and powders were investigated with the aim of studying the interaction of the guest clusters with the host silica matrix and to verify whether the distribution of the guest oxoclusters in the starting hybrid materials is retained also upon calcination.

2. Results and Discussion

The prepared samples were characterized both as-prepared and after thermal treatment to investigate the effect of the temperature on their compositional, microstructural, and morphological features. IR spectroscopy was used to investigate the composition of the samples containing both zirconium and hafnium clusters before and after calcination.

In Figure 1a and b the IR spectra of the sample SiZrHf10-f before (Fig. 1a), and after calcination (Fig. 1b) are compared. The detected peaks were assigned according to the values reported in literature[15,45–47] and the main vibrational bands are evidenced and labeled in Figure 1a and b. The typical vibrations of silica are well evident in the as-prepared samples as outlined by the bands at ca. 780 cm^{-1} and at 1100 cm^{-1}, ascribed to the symmetric and asymmetric stretching of the Si–O–Si group, respectively.[47] There is no evidence of vibrations corresponding to Si–O–Zr or Si–O–Hf, which should occur at 980 cm^{-1}.[15,48] Upon calcination, the band ascribed to the Si–O–Si asymmetric stretching is shifted to a lower wavenumber, 1066 cm^{-1}.[18,49,50] A further band at 450 cm^{-1} was also detected, which has been ascribed by other authors to the vibrations of the Si–O–Si network.[8]

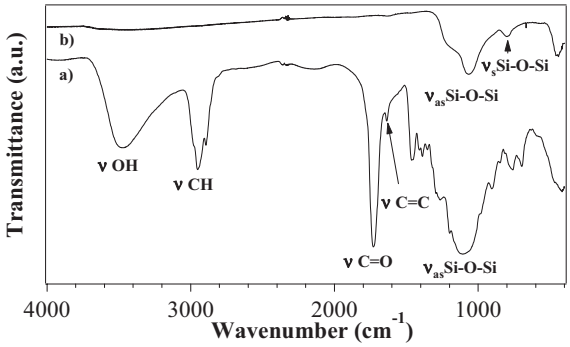

Figure 1. Superimposed FTIR spectra of the a) as-prepared and b) calcined SiZrHf10-f film samples.

All vibrations typical of the organic components of the matrix could be detected in the as-prepared samples. The bands at 2890 and 2950 cm^{-1} are due to the asymmetric stretching of $\nu_s(CH_3)$ groups and to the symmetric $\nu_s(CH)$ stretching of the terminal methylene double bonds (=CH_2), respectively.[8] Accordingly, all these vibrational modes disappeared upon calcinations. The sharp band at 1730 cm^{-1} is ascribed to the C=O carbonyl group. Due to the hampered mobility of the methacrylate groups, which are covalently linked to the already partially formed silica network and also to the steric restrictions imposed by the two isostructural clusters, both bearing twelve methacrylate groups, a complete copolymerisation of the cluster methacrylate groups with the methacryloxysilane could not be achieved, as evidenced by the band at 1635 cm^{-1}, attributed to the stretching of unreacted C=C bonds of the methacrylate.

In the as-prepared sample, a broad band at 3450 cm^{-1} was also detected, which originates from the contributions of the stretching vibration of the OH groups of water adsorbed and of the Si–OH groups. Accordingly, both bands disappear upon calcination. In the calcined samples, only the bands of silica at

ADVANCED FUNCTIONAL MATERIALS

1068, 804, and 450 cm^{-1} are present, while the features typical of the organic parts completely disappeared, as expected upon calcination at high temperature.

As can be seen in Figure 2a and b, the IR spectra of the SiZrHf40-p powders before and after calcination are very similar to those reported for the film. The main difference observed

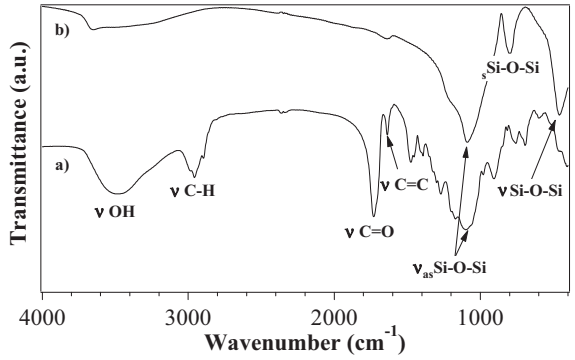

Figure 2. Superimposed FTIR spectra of the a) as-prepared and b) calcined SiZrHf40-p powder samples.

is ascribed to the presence of adsorbed water in the calcined powder, which is visible from the bands located at ca. 3600 and 1630 cm^{-1}, due to the stretching and the bending of H–O–H, respectively. The typical bands of the silica network in the as-prepared gel are located at 1100, 767, and 467 cm^{-1}, while in the calcined samples they are at 1090, 798, and 460 cm^{-1}, in accord with previous literature data. As mentioned, in both film and powder samples, the possibly of heterolinkages occurring could be not be evidenced: Si–O–M stretching would in fact be expected at about 980 cm^{-1}.[15,48]

As in the case of the binary systems,[34] despite the different sample composition and annealing, the vibrational spectroscopy outlines i) the formation of a polysiloxane network in the hybrid systems, ii) no remarkable differences between films and powders, and iii) incomplete polymerization of the methacrylate groups, likely due to steric hindrance and the limited mobility imposed by the silica matrix. The thermal heating induces a complete densification of the matrix and disappearance of the organic components.

XPS and SIMS measurements provide complementary information on the surface and in-depth composition of both the as-prepared and calcined specimens. For comparison, the surface XPS spectrum of the UV-polymerized MAPTMS (Si-f) as-prepared was also acquired. In Figure 3, the XPS survey spectra of the sample as-prepared Si-f, as-prepared SiZrHf10-f, and SiZrHf10-f calcined at 800 °C for 3 h are superimposed, while in Figure 4 the superimposed survey spectra of SiZrHf40-f as-prepared and calcined at 800 °C for 3 h are reported. In the samples without thermal treatment, the elements C, Si, O, Zr, and Hf are present. Upon calcination, due to the burnout of the organic part in the hybrid precursors, a drastic reduction of carbon content was observed. Detailed scans were acquired for the mentioned elements. In Figure 5 a typical peak of Hf4d of

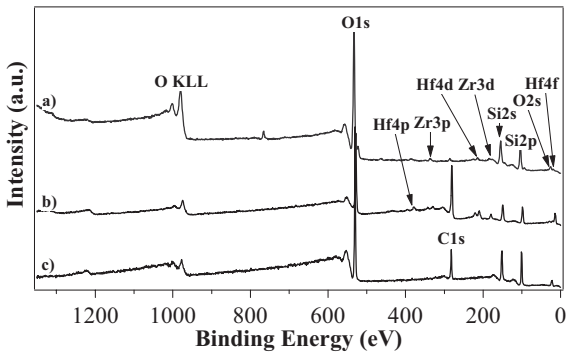

Figure 3. Superimposed XPS surveys of the SiZrHf10-f samples a) calcined and b) as-prepared, and c) the Si-f sample, as-prepared.

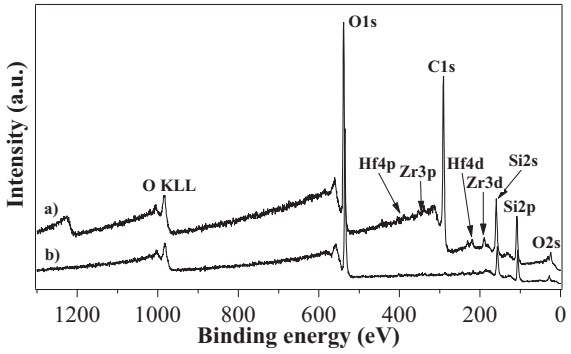

Figure 4. Superimposed XPS surveys of the a) as-prepared and b) calcined SiZrHf40-f samples.

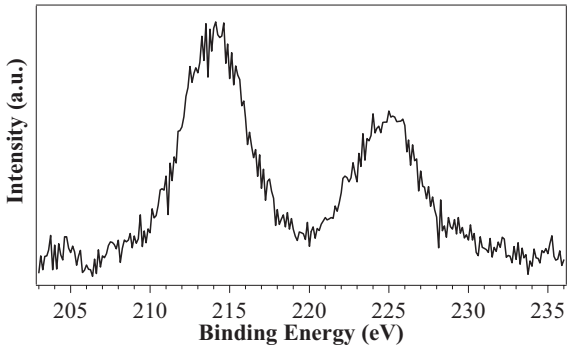

Figure 5. Hf4d XPS peak of the calcined SiZrHf10-f sample.

the sample SiZrHf10-f calcined at 800 °C is shown. Depth profiles were performed on the samples SiZrHf10-f and SiZrHf40-f before and after calcination. In all cases, the in-depth quantitative analysis showed an even distribution of the guest zirconium and hafnium-related species in both the as-prepared and calcined specimens. This can be observed in Figure 6, where the Si/Zr and Si/Hf atomic ratios in the as-prepared SiZrHf10-f sample are plotted.

As can be seen in the plots of the ratio of the atomic percentages versus time of sputtering, which can, in turn, be related to the eroded depth, the guest species are quite evenly distributed

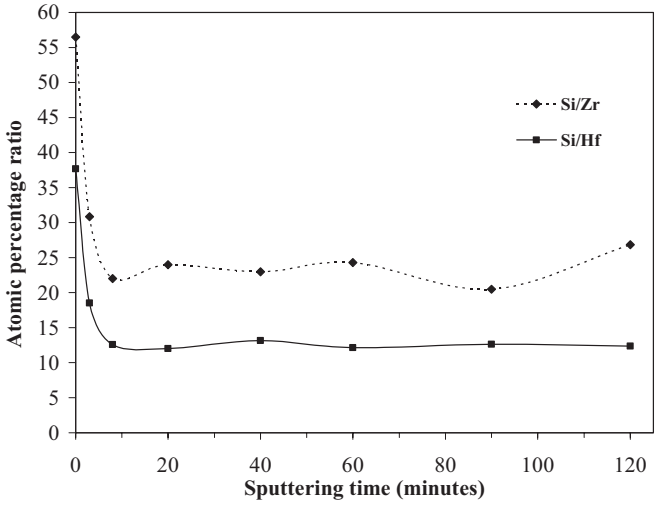

Figure 6. XPS in-depth profiles of the as-prepared SiZrHf10-p sample as a function of sputtering time.

along the whole film thickness. The even distribution is observed in both the as-prepared and calcined specimens. The calcination does not affect the distribution of the metal species in the films. A significant difference among the two sets of samples concerns the carbon content. While in the crude samples, carbon is detected in a considerable amount (50 %), in agreement with the preparative data (47 %) and with the inorganic–organic hybrid nature of the materials, a very low carbon content (< 1 %) is present after calcination.

Assuming that silicon is mostly present as silica in the calcined samples, and by giving the Si2p the value of SiO_2, that is, 103.6 eV,[51] the corrected binding energy (BE) of $Zr3d_{5/2}$ has a value of 183.6 eV for the calcined SiZrHf10-f sample, a value higher than bulk zirconium oxide, 182.2 eV.[51] This finding can be rationalized by considering that, in a system consisting of zirconia particles dispersed in a silica matrix, zirconium experiences a chemical environment that is substantially different from that in bulk zirconia. In fact, silicon is more electronegative than zirconium and the Si–O– bonds around Zr are expected to withdraw more electron density than a Zr–O environment, which would be expected in the case of a pure zirconium oxide. This implies a shift of the Zr3d BE towards higher BEs as the value of 183.1 eV of the Zr3d peak already reported for zirconia–silica binary systems characterized by a zirconia amount < 20 wt %.[33,34,52] In particular, in the present study, the shift to a higher value is ascribed to the smaller relaxation energy of the highly dispersed zirconium oxide species compared to the powdered ZrO_2. Analogous considerations can be extended to the shifted BEs observed in the case of hafnium.

A further insight on the in-depth distribution of zirconium and hafnium species in the silica matrix along the whole film thickness was obtained by performing SIMS analysis. In this case, samples prepared by spin-coating (SiZrHf40-f) were compared with the sample prepared by dip-coating (SiZrHf10-f*). In Figure 7a and b the element SIMS profiles of sample

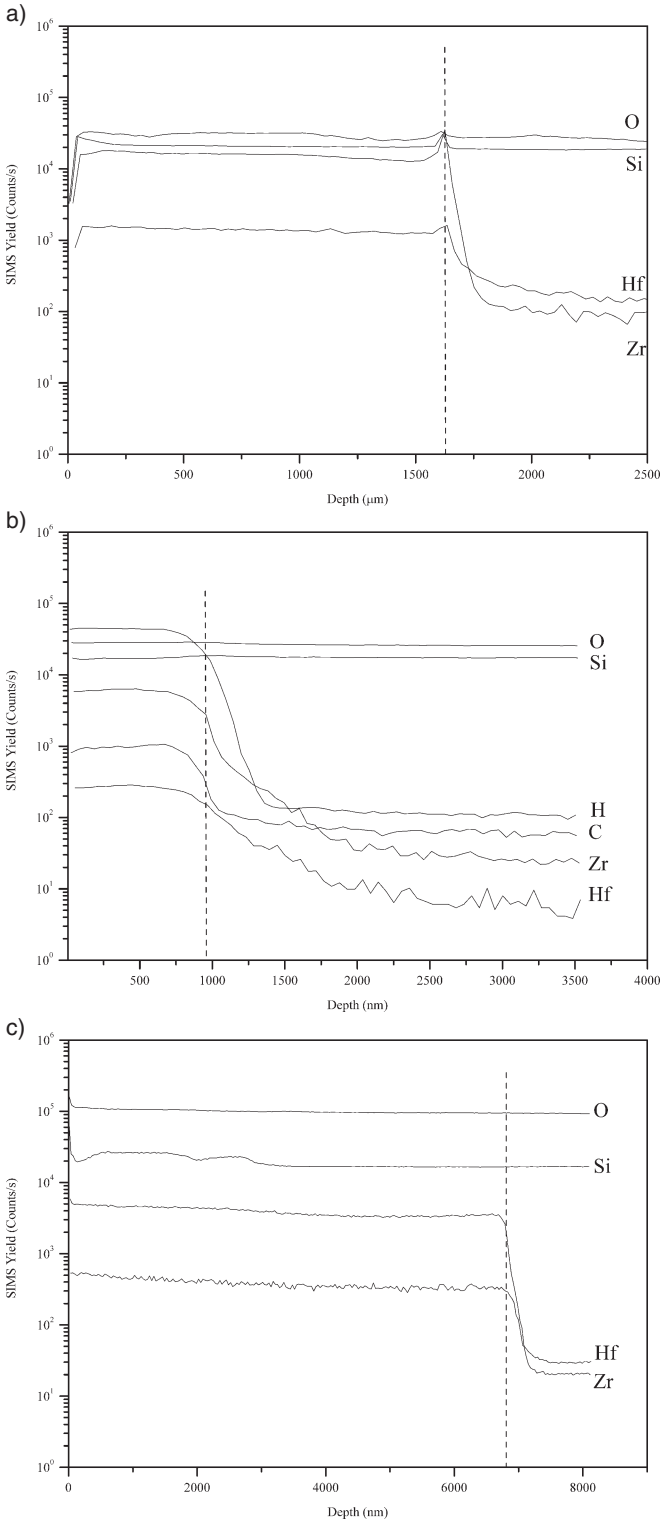

Figure 7. SIMS profiles of the SiZrHf10-f samples deposited by dip-coating a) as-prepared sample, b) calcined sample at 800 °C for 3 h, c) as-prepared SiZrHf40-f sample deposited by spin-coating.

SiZrHf10-f* and SiZrHf10C-f*, respectively, are reported. The films thickness was estimated to be ca 1.6 μm in the as-prepared sample; it was considerably reduced after calcination,

(ca. 0.9 μm). The film-to-substrate interface is sharp in the as-prepared sample, the element interdiffusion is limited to a thickness lower than 200 nm, while it increases significantly after the calcination process.

In Figure 7c the element SIMS profiles of the spin-coated SiZrHf10-f sample are reported. The film thickness was found to be close to 6.2 μm in the as-prepared sample and close to 1.4 μm after the calcination process. The film-to-substrate interface is sharp, the element interdiffusion is limited to a thickness below 100 nm in the as-prepared sample but increases up to 350 nm after the calcination.

The most remarkable difference between the sample prepared by dip-coating and that prepared by spin-coating is the shrinkage upon annealing, which can be in turn traced back to the thickness of the films, which is noticeably higher in the case of spin-coated samples. Furthermore, whereas in the case of layers deposited by dip-coating, the homogeneous distribution of the species detected in the as-prepared sample (see Fig. 7a–c) is retained after calcination, in the case of spin-coated films, a dramatic thinning and the cracking of the layers was observed after calcination which can be again ascribed to the higher shrinkage of the thicker films. Complementary information on the system composition was achieved by using laser ablation inductively coupled plasma mass spectrometry (LA-ICPMS), which was used to investigate the sample composition on a lateral distribution. Figure 8 shows the Si/(Zr+Hf) ratios in a series of samples of different composition, before and after thermal annealing. As evidenced by the bars, the found atomic ratios are in agreement with those in the starting precursor solution. Furthermore, as expected, these atomic ratios do not change upon annealing, and they remain practically unchanged in the calcined samples (labeled as "calc" in Fig. 8). The lateral homogeneity in all the samples is quite good, with a relative standard deviation (RSD) of about 10 % (i.e., 7–11 %) for all samples, except for calcined SiZrHf10-f (15 %). These findings, taking also into account the limits associated with LA-ICPMS determinations, evidences a good lateral compositional homogeneity showing that Hf and Zr are mostly concentrated in the first hundreds of nanometers beneath the surface, in agreement with SIMS results.

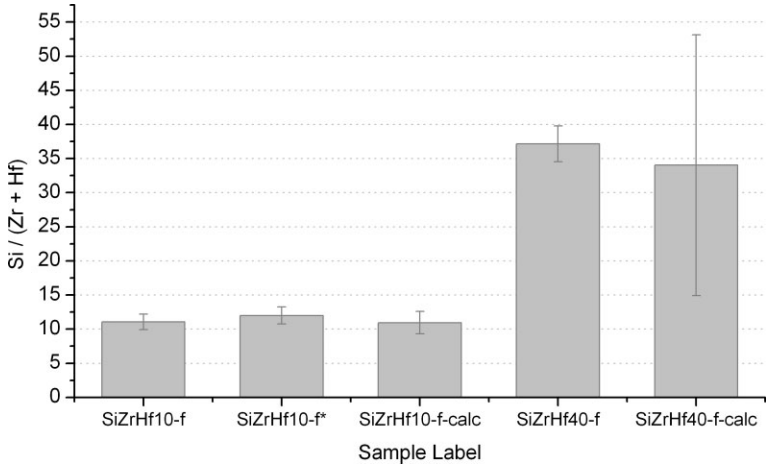

Figure 8. Si/(Zr+Hf) atomic ratio for the set of prepared thin films, as obtained from LA-ICPMS determinations. The additional labeling "calc" indicates a calcinated sample.

The microstructure of the powders and of the film was studied by conventional and grazing-angle X-ray diffraction, respectively. This latter method was adopted to minimize the contribution of the silica substrate. The as-prepared specimens and the samples calcined at 800 °C present a featureless XRD pattern, characterised only by the presence of the 21.5° broad band, of amorphous silica (not shown in Fig. 9).[53] The lack of diffraction reflections can be either ascribed to the presence of amorphous phases or to very small nanocrystallites (< 3 nm),

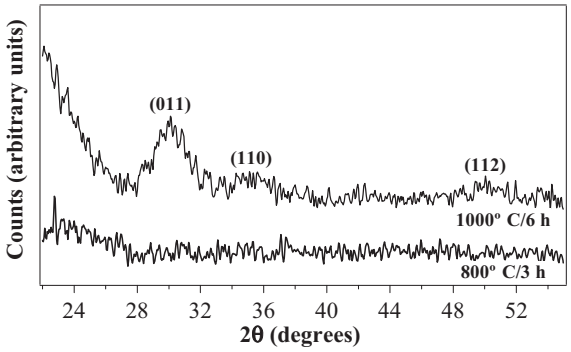

Figure 9. XRD patterns of the SiZrHf10-f sample treated at 800° C for 3 h and at 1000 °C for 6 h.

or to the concurrence of both phenomena. Only after calcination at 1000° C were diffraction reflections observed (Fig. 9). The most intense peak at $2\theta = 21.5°$ is due to silica (not shown in Fig. 9), while the broad reflections at 30.2° (011), 35.5° (110), and 50.5° (112) are ascribed to tetragonal ZrO_2. A second thermal treatment at 1000 °C for 5 h does not remarkably change the diffraction pattern.

As already observed in the case of zirconia–silica and hafnia–silica, also in this ternary system, crystallization occurs at a temperature higher than that expected for pure hafnia or zirconia.[45] This phenomenon, which occurs whenever zirconia or hafnia are homogeneously dispersed in a silica matrix, has been extensively described in the literature.[7,54–62] Generally, the crystallization of tetragonal zirconia has been reported to occur after calcination at 400 °C,[15] while partial transformation from tetragonal to monoclinic was reported to occur at 800–900 °C and the single monoclinic phase is present at temperatures higher than 1000–1200 °C. However, Neumayer and Cartier[15] reported that the addition of silica to zirconium and hafnium oxide was found to increase the temperature of crystallization of zirconium oxide, to stabilize the formation of tetragonal hafnia, and to increase the temperature at which the transformation of ZrO_2 or HfO_2 from the tetragonal to the monoclinic phase occurs. Whenever zirconia or hafnia are homogeneously dispersed in a silica matrix, the crystallization requires both diffusion as well as grain growth, and a correlation be-

tween this delayed crystallization and the homogeneity of the materials has been established.[62]

As already evidenced in our previous works,[33–35] the in-depth distribution at different length scales of the host species evidenced by XPS and SIMS depth profiles could be traced back to the formation of well-distributed guest clusters in the host matrix. Also in the present case, the presence of isolated clusters was demonstrated by transmission electron microscopy (TEM) images. In Figure 10, the TEM images of the SiZrHf10-p sample calcined at 1000 °C for 6 h, are reported, while TEM images of the samples SiZrHf10-f and SiZrHf40-f, both calcined at 1000 °C for 6 h, are reported in Figures 11 and 12.

In the SAED of samples SiZrHf10-p and SiZrHf10-f, two sets of patterns can be distinguished: one corresponding to the nanoparticles consisting of the binary oxide (Zr, Hf)O_2 and one corresponding to the silica matrix. The (111) reflection of (Zr, Hf)O_2 is in good agreement with the literature value

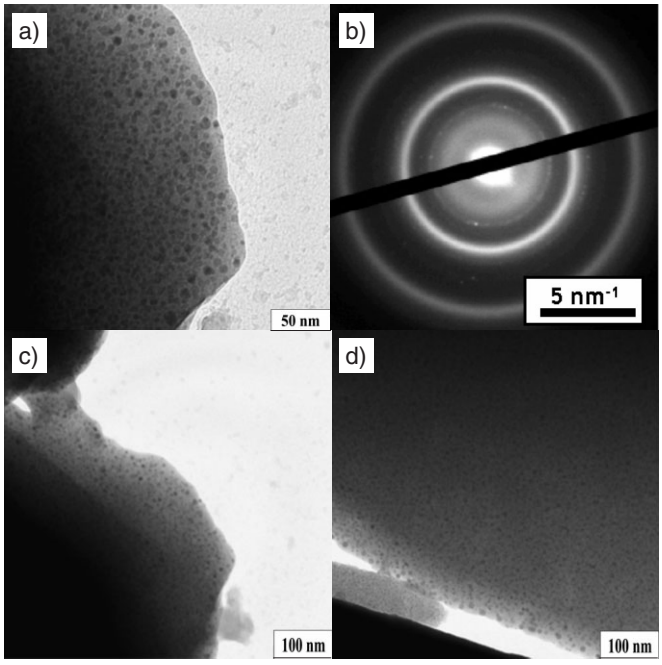

Figure 10. a,c,d) TEM images and b) corresponding SAED pattern of the calcined SiZrHf10-p sample at 1000 °C for 6 h.

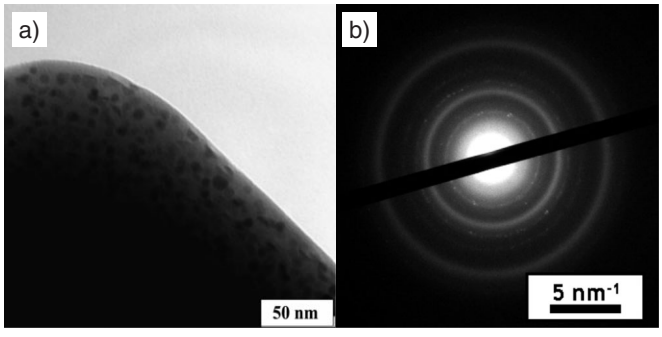

Figure 11. a) TEM image and b) corresponding SAED pattern of the sample SiZrHf10-f calcined at 1000 °C for 6 h.

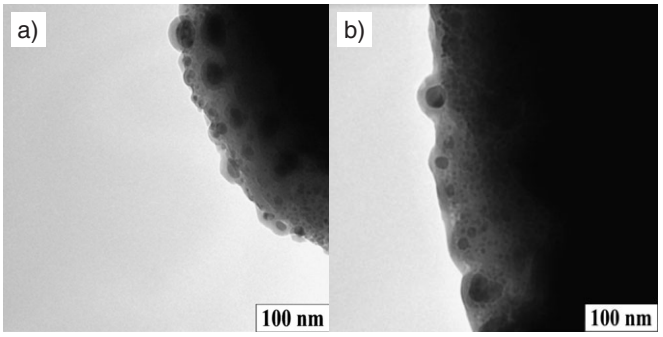

Figure 12. a,b) TEM images of the sample SiZrHf40-f calcined at 1000 °C for 6 h.

(ca. 2.9 Å), whereas the strong broad reflections arise from the amorphous silica matrix. It should be pointed out that film and powders of the same composition show a very similar microstructure characterised by an even distribution of isolated nanoclusters with a diameter ranging from 5 to 10 nm. The presence of crystalline nanoparticles of hafnia and zirconia in the samples SiZrHf10-p and SiZrHf10-f, respectively, was proved by using electron diffraction (data not shown). It was not possible to index the complete set of reflections of (Zr, Hf)O_2, owing to the relative low intensity of the pattern, demonstrating the low relative content of both elements within the siliceous matrix. From the SAED pattern alone it could not be determined whether a mixed oxide or both oxides have been formed simultaneously, since the main reflections of ZrO_2 and HfO_2 are very close.

However, the formation of mixed oxides between Zr and Hf is well known in chemistry, since Zr and Hf are chemically very similar elements, that is, they have the same ionic radius. On the basis of these findings, the formation of a mixed oxide homogeneous on a molecular level can be hypothized. It has to be underlined that the SiZrHf40-f sample, calcined at 1000 °C for 6 h, characterised by a lower concentration of zirconia, shows some agglomeration, leading to some coalescence of the nanoparticles: in this case, an average diameter of about 25–30 nm was observed. On the contrary, these agglomeration phenomena are not pointed out in the more diluted sample containing hafnia clusters.

To better investigate the local structural order as well as the possible mutual interaction of the oxides and their interaction with the surrounding host silica matrix, X-ray absorption fine structure (XAFS) analysis was carried out on the SiZrHf10-p sample calcined at 800 °C for 3 h, at both Zr K and Hf L_{III}-edges. The experimentally determined and theoretically calculated extended XAFS (EXAFS) functions of SiZrHf10-p measured at the Hf L_{III} edge are shown in k space as well as by Fourier transforms in real space in Figure 13 and the corresponding structural parameters are summarized in Table 1. In the fitting procedure, the various parameters, that is, coordination number, interatomic distance, Debye-Waller factor, and energy zero value were determined by iterations. In the analysis of the experimental k^3-weighed $\chi(k)$ function, a three-shell model can be fitted for SiZrHf10-p measured at the Hf L_{III}-edge. The

ADVANCED FUNCTIONAL MATERIALS

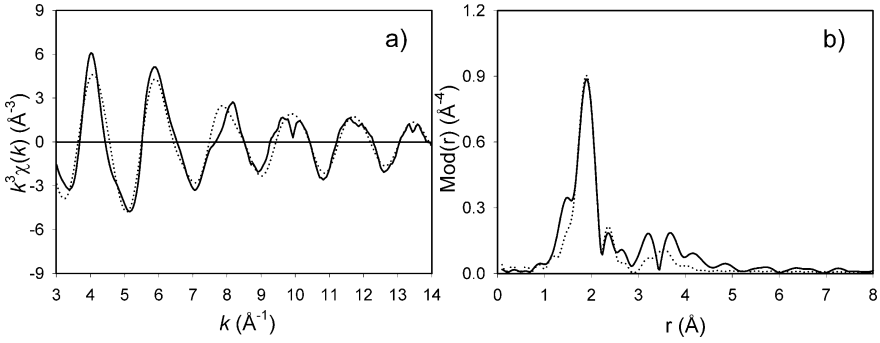

Figure 13. a,b) Experimental (solid line) and calculated (dotted line) EXAFS functions and their corresponding Fourier transforms of SiZrHf10-p measured at the Hf L_{III}-edge.

Table 1. EXAFS determined structural parameters of SiZrHf10-p.

Absorption edge	A–Bs [a]	*N* [b]	*r* [c] [Å]	σ [d] [Å]	ΔE_0 [e] [eV]	*k* range [Å^{-1}]	Fit index
	Hf–O	4.1 ± 0.4	2.00 ± 0.02	0.071 ± 0.007	13.56	3.0–14.0	30.56
Hf L_{III}-edge	Hf–O	2.2 ± 0.2	2.20 ± 0.02	0.077 ± 0.009			
	Hf–Hf	2.3 ± 0.3	3.45 ± 0.04	0.122 ± 0.016			
	Zr–O	3.8 ± 0.4	2.01 ± 0.02	0.071 ± 0.007	18.72	3.0–10.0	46.68
Zr K-edge	Zr–O	5.6 ± 0.6	2.22 ± 0.02	0.105 ± 0.011			
	Zr–Zr	2.0 ± 0.3	3.28 ± 0.04	0.107 ± 0.014			

[a] Absorber–backscatterers. [b] Coordination number *N*. [c] Interatomic distance *r*. [d] Debye–Waller factor σ with its calculated deviation. [e] Shift of the threshold energy ΔE_0).

first shell consists of about 4.1 oxygen backscatterers at 2.00 Å, the second shell comprises of about 2.2 oxygen backscatterers at 2.20 Å and the third shell has about 2.3 hafnium backscatterers at 3.45 Å distance. The obtained structural parameters are in very good agreement with those reported for a similar sample (SiHf17 calcined at the same temperature) in an earlier work.[35] As the sample was predominantly amorphous, it was not possible to match the EXAFS-determined values with any of the well-known polymorphs of HfO_2. Furthermore, distances corresponding to Hf–O–Si mixed bonds could not be evidenced by using EXAFS analysis. Analogously, the experimentally determined and theoretically calculated EXAFS functions of SiZrHf10-p measured at the Zr K-edge are shown in *k* space as well as by Fourier transforms in real space in Figure 14, and the structural parameters are given in Table 1.

Due to the low absorption jump at the Zr K-edge owing to the high extinction, the signal-to-noise ratio was low in the measured spectrum and the EXAFS spectrum could be evaluated only to the 10 Å^{-1} *k* range. In this fitting procedure, coordination number, interatomic distance, Debye–Waller factor, and energy zero value were determined by iterations. In the analysis of the EXAFS function, a three-shell model comprising of two oxygen shells and one zirconium shell could be fitted for SiZrHf10-p. The first shell at 2.01 Å distance with about 3.8 backscatterers, the second shell at 2.22 Å distance with about 5.6 backscatterers, and the third shell at 3.28 Å distance with about 2.0 backscatterers were determined. In addition, distances corresponding to Zr–O–Si or Zr–O–Hf mixed bonds could not be evidenced by using EXAFS analysis and the determined structural parameters could not be matched with any of the well-known polymorphs of crystalline ZrO_2. In this regard further information was obtained from the X-ray absorption near-edge structure (XANES) region.

A comparison of the XANES spectrum of SiZrHf10-p with those of the pureZr4 cluster and the reference ZrO_2 polymorphs is shown in Figure 15. For reasons of clarity, the XANES regions of different samples are shifted along the ordinate. It could be observed that the SiZrHf10-p was similar to that of the tetragonal polymorph, characterized by the presence of a twin peak over the absorption edge. This information was further strengthened by the XRD investigations on the sample calcined at 1000 °C, which indicated the presence of tetragonal zirconia.

3. Conclusions

Ternary ZrO_2–HfO_2–SiO_2 film and bulk materials of different compositions were prepared by using a modified sol–gel procedure based on the use of a bifunctional siloxane and Hf- and Zr-oxoclusters as molecular building blocks (see Figure 16). The adopted approach enabled the attainment of a homogeneous distribution of the two guest oxides in the host silica matrix and to favor the formation, upon annealing, of well-dispersed nanometer-sized clusters. An even distribution of the guest oxides within the whole thickness of the host silica

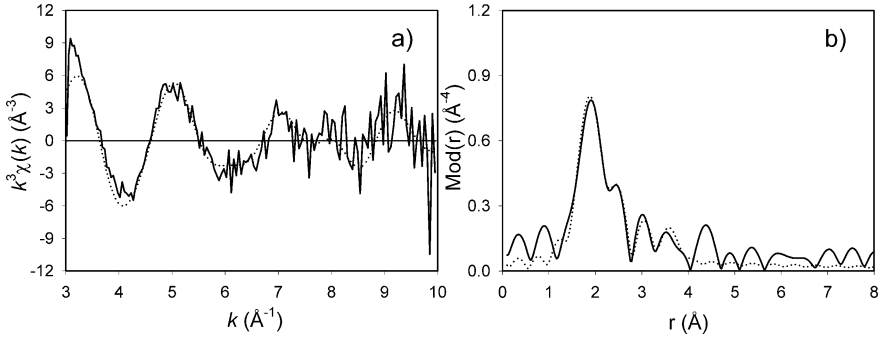

Figure 14. a,b) Experimental (solid line) and calculated (dotted line) EXAFS functions and their corresponding Fourier transforms of SiZrHf10-p measured at the Zr K-edge.

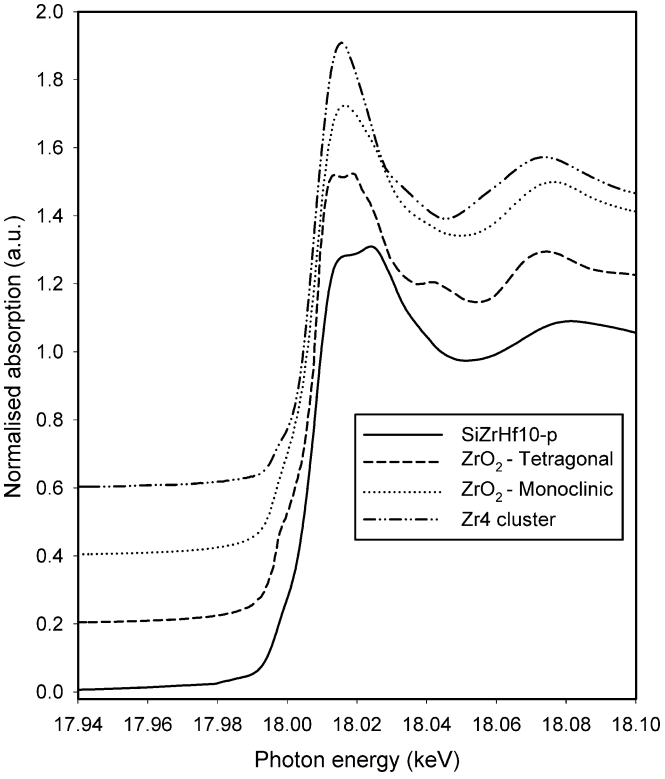

Figure 15. XANES region of SiZrHf10-p, pure Zr4 cluster, and the reference ZrO_2 polymorphs.

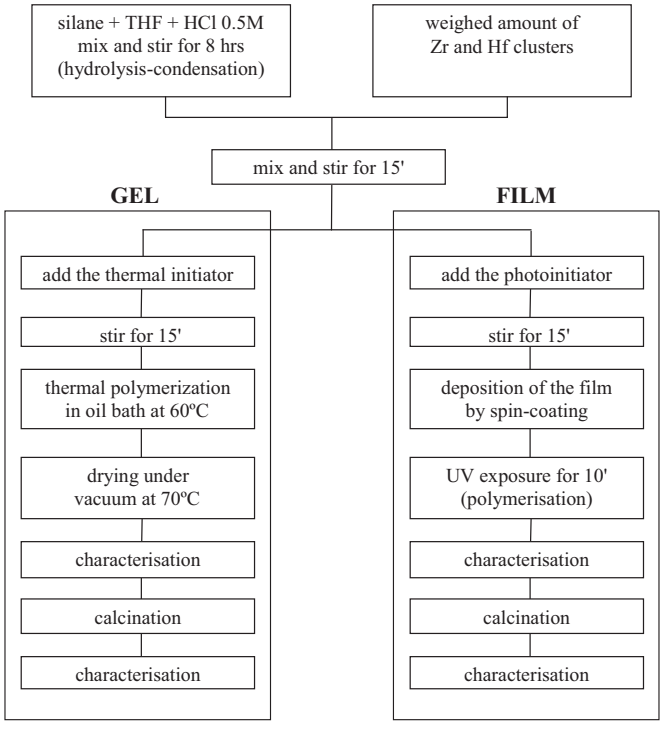

Figure 16. Flow chart of the synthetic procedure for the preparation of films and gels.

layers was evidenced by XPS and SIMS in-depth profiles, while a good lateral distribution could be assessed by using LA-ICPMS.

The homogeneous distribution would also explain the higher crystallization temperature of the crystalline phase evidenced by XRD measurements. The formation of isolated crystalline clusters of zirconia and hafnia was confirmed from TEM images. The average size of the crystallite is about 5 to 10 nm.

The Hf L_{III} edge and Zr K-edge XAFS measurements on SiZrHf10-p indicate that the sample is predominantly amorphous and that the oxide structure has not completely formed when the sample is calcined at 800 °C. However, the XANES spectrum at the Zr K-edge resembles that of tetragonal zirconia, which is formed when the sample is calcined at higher temperatures, as evidenced by XRD data. The formation of Hf–O–Si, Zr–O–Si, or Zr–O–Hf mixed bonds was not evidenced.

In conclusion, the grafting of the cluster (molecular precursor for the guest oxides) to the bifunctional silane (precursor for the host matrix) and the subsequent calcination at high temperature was demonstrated to represent an effective approach to achieve highly dispersed ZrO_2-HfO_2 nanoparticles in silica glass. It should, moreover, be highlighted that the versatility of this approach, which allows, depending on the adopted synthesis procedure and calcination temperature, i) the attainment of either amorphous or crystalline materials; ii) the preparation of the mentioned systems both as thin films and in the form of powders (massive materials), and iii) the embedding of different amounts of the guest Zr and Hf oxides in the host silica matrix.

This, in turn, enables the envisagement of different applications for these mixed oxide materials ranging from optics (Zr and Hf oxides embedded in silica change its refractive index), to electronic applications for the thin films, to catalysts for powders. It has been in fact demonstrated that an even dispersion of zirconia or hafnia nanoparticles in a silica matrix strongly increases its activity in catalytic reactions such as isopropanol and *n*-butanol dehydration and cycloesanol dehydrogenation.[63]

4. Experimental

Chemicals: MAPTMS and $Hf(OBu)_4$ were purchased from ABCR, Karlsruhe, Germany; anhydrous tetrahydrofuran and anhydrous toluene, $Zr(OBu)_4$ and dibenzoylperoxide were all purchased from Aldrich. Methacrylic acid 99 %, purchased from Aldrich, was distilled under reduced pressure. All the chemicals were stored under argon, while the solvents were additionally stored on molecular sieves. The photoinitiator Irgacure 184 (I184, 1-hydroxycyclohexyl-1-phenylketone) was received as a gift by Ciba Specialty Chemicals, Basel, Switzerland. The $M_4O_2(OMc)_{12}$ clusters were synthesized starting from the corresponding alkoxides by a previously reported procedure [39,40].

Precursor Solutions: All handlings were performed under argon using standard Schlenk techniques. The preparation of the starting solution used for film deposition can be described as a three-step process, as sketched on the right side of the flow chart in Figure 1. For the preparation of the powders a similar procedure was adopted (left side of the flow chart in Fig. 1), but in this case a thermal polymerization instead of a photopolymerization was used to achieve bulk inorganic–organic hybrid materials.

First, MAPTMS was dissolved in anhydrous tetrahydrofuran and prehydrolyzed with water in the presence of HCl as a catalyst for 8 h at room temperature. The typical composition of the sol–gel solution is 1 silane:4 H_2O:0.04 HCl molar ratio. The hydrolysis time was chosen on the basis of time-resolved IR studies of the hydrolysis rate of the silane. A calculated amount of the crystalline clusters was mixed with the solution of the prehydrolyzed silane and stirred at room temperature for 15 min. Different solutions characterised by different Si/(Zr+Hf) molar ratios were prepared, as reported in Table 2.

Table 2. Composition and labeling of the samples.

Sample	Si/(Zr+Hf) molar ratio
Si-p	without clusters
SiZrHf20-p	20
SiZrHf10-p	10
SiZrHf40-p	40
Si-f	without clusters
SiZrHf10-f	10
SiZrHf40-f	40

To this solution, CIBA Irgacure 184 was added 1 wt % (with respect to silane) as a radical photoinitiator under stirring. When excited to its triplet state by using UV radiation, the molecule undergoes α-cleavage to produce benzoyl and 1-hydroxycyclohexyl radicals. The former is primarily responsible for initiating the polymerization of the methacryloxypropyl group. Bulk powders were prepared starting from the solutions prepared as those used for the films and by using thermal initiated polymerization. To the solution the initiator dibenzoylperoxide was added (1 wt % with respect to the silane monomer) under stirring. The obtained solutions were heated at 60 °C until polymerization occurred. A typical polymerization time was about 1 h. Table 2 summarizes the different molar ratios used for the preparation of the samples, according to the nominal composition of the solution. In Table 2 and in the following, the labels "SiZrHf number" indicate the specimens prepared by using the zirconium and hafnium oxoclusters, whereas the number indicates the Si/(Zr+Hf) atomic ratio. The Hf/Zr molar ratio was kept constant at one. The label "p" or "f" indicates the powder or film samples, respectively. The film samples labeled with a star were prepared by using a dip-coating deposition. Finally, the label "Si" indicates the samples without clusters, used as a reference. The label "c" indicates calcined samples.

Film Deposition and UV Curing: The films were prepared via a spin-coating procedure using a spin coater model 6708D 8″ "Desktop precision spin-coating system". Two different materials were used as substrates: silicon wafers (Si(110)) and Herasil silica slides, supplied by Hereaus. Before use, the slides were cleaned and rinsed both in doubly distilled water and 2-propanol. This procedure was repeated several times to remove organic residuals at the surface, thus favoring the best adhesion between the coating and substrate. The slides were finally dried in air at room temperature [64]. A solution of precursors was dropped on the centre of the slide; successively, the rotating rate was progressively increased to 3000 rpm and this rotating rate was maintained for 30 s. Transparent and homogeneous films were obtained with a thickness of ca. 6–7 μm. A selected sample (SiZrHf10-f*) was also prepared by using a dip-coating procedure, in order to test the effect of deposition procedure on the final features of the films. In this case, film deposition was carried out in air at a constant withdrawal speed of 10 cm min^{-1}, at room temperature with a relative humidity of 30–40 % by using homemade equipment.

As a reference, the MAPTMS silane without the addition of hafnium or zirconium clusters was also cast into a film and UV cured. After spin(dip)-coating, the films were irradiated under an UV source for 10 min to promote the polymerization of methacrylate. The irradiation time was optimized on the basis of time-dependent IR measurements, as already reported [34]. The irradiation source was a Helios Italquartz s.r.l. lamp with a power of 125 W and an emission range of 250–450 nm. The as-prepared films were transparent, crack-free, uniform, and smooth, without any agglomeration on their surface. They were subsequently calcined in air at 800° C for 3 h to remove the organic groups and to yield the final mixed oxides. Homogeneous and well-adherent films were obtained on all the substrates. Some selected samples were also calcined at 1000 °C for 6 h to investigate their crystallization behavior. Transparent and smooth films were obtained. As a general trend, a thinning of the samples upon calcination was observed, which can be ascribed to the densification of the films and to the burnout of the organic parts. For some selected samples, the thickness was determined by measuring the crater depth made after the SIMS analysis by using a Tencor Alpha Step profilometer. The determined values for some selected as-prepared samples are reported in Table 3, where the error on the thickness determination contains the contribution of the surface roughness and the profilometer scan error.

Table 3. Thickness of some selected films.

Sample	Thickness FWHM [nm] as prepared
SiZrHf10	7620 ± 251
	6160 ± 102
SiZrHf10*	1650 ± 122
SiZrHf40	6887 ± 163

Film and Powder Characterization: FTIR analyses spectra were recorded in transmission with a Nexus 870 FTIR spectrometer (Nicolet) in the 400 to 4000 cm^{-1} range, by using a resolution of 4 cm^{-1}. The films for the analysis were spun onto a one-side-polished Si wafer. The solid samples were finely ground and analyzed by dispersing them into pellets of spectroscopic-grade potassium bromide (purchased from Aldrich), which was previously anidrified in vacuum at 150 °C for 24 h.

The composition of the films at the surface and in the bulk was investigated by using XPS. Photoelectron spectra were run on a Perkin–Elmer Φ5600ci spectrometer using non-monochromatized Al Kα radiation (1486.6 eV). The working pressure was $< 5 \times 10^{-8}$ Pa. The spectrometer was calibrated by assuming the BE of the $Au4f_{7/2}$ line at 83.9 eV with respect to the Fermi level. The standard deviation for the BE values was 0.15 eV. The reported BE were corrected for the charging effects, assigning to the C 1s line of adventitious carbon the BE value of 285.0 eV [65]. In the calcined samples, in which no carbon could be detected, charging effects were corrected by assuming for the Si2p peak a BE value typical of silicon in silica, that is, 103.6 eV. This implies the assumption that silicon experiences mostly a silica environment. Considering that, also in the most concentrated sample, the amount of silica is at least 80 at this assumption can be considered reliable in a first approximation. Survey scans were obtained in the 0–1350 eV range. Detailed scans were recorded for the O 1s, Si 2p, Zr 3d, Zr 3p Hf 4f, Hf 4d, and C 1s regions. The atomic composition was evaluated using sensitivity factors supplied by Perkin–Elmer [51]. Depth profiles were carried out by Ar^+ sputtering at 3 kV with an argon partial pressure of 5×10^{-6} Pa. A specimen area of 2 mm × 2 mm was sputtered. A flood gun was used to compensate charging effects on the surface of the irradiated specimens. Samples were introduced directly, by a fast entry lock system, into the XPS analytical chamber.

XRD data were collected with a Bruker D8 Advance Diffractometer equipped with a Göbel mirror and a Cu Kα source (40 kV, 40 mA). The angular accuracy was 0.001° and the angular resolution was better than 0.01°. Glancing incidence patterns were recorded at a fixed incidence angle of 1.5°. The average crystallite size was calculated from the most-intense diffraction peaks by means of the Scherrer equation.

LA-ICPMS is based on laser-assisted microsampling and transport of the laser-induced aerosol to a plasma-source mass spectrometer, by means of a carrier gas. LA-ICPMS measurements were performed using an in-house redesigned Nd:YAG (YAG: yttrium aluminum gar-

net) laser ablation system (Quanta-Ray DCR-11, Spectra-Physics) operating at the fourth harmonic (266 nm) for improved ablation characteristics. The laser was pulsed at 10 Hz, with a pulse energy of 4 mJ. The laser beam was focused with a $f = 40$ mm plano-convex lens. A pinhole was used to collimate the beam onto the sample surface and adjust the spot size. The ablation cell was 30 cm^3 with an inlet nozzle of 0.5 mm inside diameter (i.d.) to ensure a steady gas jet. The transport tube was a 4 mm i.d. and 1.5 m long PVC tube. Helium was used as a carrier gas at a flow rate of 0.6 $L\,min^{-1}$. The ICP mass spectrometer was a quadrupole plasma-mass spectrometer (PE/Sciex Elan 6000) operated under standard conditions.

SIMS measurements were carried on a IMS 4f mass spectrometer (Cameca, Padova, Italy) using a 10 kV Cs^+ primary beam and by negative secondary ion detection (the sample potential was fixed at –4.5 kV) with a final impact energy of 14.5 keV. The SIMS measurements were carried out in ultrahigh vacuum conditions at different primary beam intensities (in the range 30–50 nA) rastering over a nominally 125 μm × 125 μm area. A beam-blanking mode was used to improve the depth resolution, interrupting the sputtering process during magnet-stabilization periods. The measurements were performed in high-mass resolution configuration to avoid mass-interference artefacts. The charge build-up occurring in insulating samples during the in-depth profiling was compensated for by an electron gun without any need to cover the surface with a metal film. The erosion speed was evaluated by measuring the depth of the erosion crater at the end of each analysis by means of a Tencor Alpha Step profilometer with a maximum uncertainty of a few nanometers. The dependence of the erosion speed on the matrix composition was taken into account for each sample by recording various spectra at different depths in each sample.

TEM images were taken using a Zeiss EM 912 microscope at an acceleration voltage of 120 kV. For the films, the samples were scraped off from the substrate with a razor blade and brought onto a 400 mesh carbon-coated copper grid. Different areas were investigated in order to check the homogeneity of the material.

The XAFS measurements on SiZrHf10-p calcined at 800 °C in air for 3 h were performed at Hf L_{III}-edge at 9561 eV and Zr K-edge at 17 998 eV at the beamline X1.1 of the Hamburger Synchrotron Radiation Laboratory (HASYLAB) at DESY, Hamburg. The positron energy in the ring was 4.45 GeV and the beam current was ca. 120 mA. The samples were measured with a Si(111) double-crystal monochromator at the Hf L_{III}-edge and with a Si(311) double-crystal monochromator at the Zr K-edge. Data were collected in transmission mode with ion chambers filled with nitrogen for Hf L_{III}-edge measurements and argon for Zr K-edge measurements. Energy calibration was monitored using a 20 μm thick metal foil of the respective element. The sample in the solid state was embedded in a polyethylene matrix and pressed into a pellet. The concentration of the solid sample was adjusted to yield an extinction of 1.5. The data were analyzed with a program package developed for the evaluation of amorphous samples [66]. The program AUTOBK [67] was used for the removal of the background and the program EXCURV92 [68] was used for the evaluation of the EXAFS function. Curved wave theory was used for the data analysis in k space and the resulting EXAFS function was weighted with k^3. The mean free path of the scattered electrons was calculated from the imaginary part of the potential (VPI; set to –4.00), the amplitude factor (AFAC) was fixed at 0.8 and an overall energy shift ΔE_0 was introduced to give a best fit to the data.

Received: May 26, 2006
Revised: July 20, 2006
Published online: May 29, 2007

[1] R. G. Simhan, *J. Non-Cryst. Solids* **1983**, *54*, 335.
[2] A. Paul, *J. Mater. Sci.* **1977**, *12*, 2246.
[3] Y. S. Lin, R. Puthenkovilakam, J. P. Chang, *Appl. Phys. Lett.* **2002**, *81*, 11.
[4] G. D. Wilk, R. M. Wallace, J. M. Anthony, *J. Appl. Phys.* **2000**, *87*, 484.
[5] G. D. Wilk, R. M. Wallace, *Appl. Phys. Lett.* **1999**, *74*, 2854.
[6] G. D. Wilk, R. M. Wallace, *Appl. Phys. Lett.* **2000**, *76*, 112.
[7] J. P. Maria, D. Wickaksana, J. Parrette, A. I. Kingon, *J. Mater. Res.* **2002**, *17*, 1571.
[8] K. Saravanamuttu, D. Xin Min, S. I. Najafi, M. P. Andrews, *Can. J. Chem.* **1998**, *76*, 1717.
[9] M. Itoh, H. Hattori, K. J. Tanabe, *J. Catal.* **1974**, *35*, 225.
[10] J. B. Miller, E. I. Ko, *J. Catal.* **1996**, *159*, 58.
[11] Z. T. Feng, W. S. Postula, C. Erkey, C. V. Philip, A. Akgerman, R. G. Anthong, *J. Catal.* **1994**, *148*, 84.
[12] T. Lopez, T. Tzompantzi, J. Navarrete, R. Gomez, J. L. Boldù, E. Munoz, O. Novaro, *J. Catal.* **1999**, *181*, 285.
[13] H. J. M. Bosman, E. C. Kruissink, J. Vanderspoel, F. Vandenbrink, *J. Catal.* **1994**, *148*, 660.
[14] S. Soled, G. B. McVicker, *Catal. Today* **1992**, *14*, 189.
[15] D. A. Neumayer, E. Cartier, *J. Appl. Phys.* **2001**, *90*, 1801.
[16] C. J. Brinker, G. W. Scherer, in *Sol–Gel Science—The Physcis and Chemistry of Sol–Gel Processing*, Academic, New York **1990**.
[17] G. Mountjoy, M. A. Holland, P. Gunawidjaja, G. W. Wallidge, D. M. Pickup, R. J. Newport, M. E. Smith, *J. Sol–Gel Sci. Technol.* **2003**, *26*, 161.
[18] Z. Zhan, H. C. Zeng, *J. Non-Cryst. Solids* **1999**, *243*, 26.
[19] J. B. Miller, E. I. Ko, *Catal. Today* **1997**, *35*, 269.
[20] G. Mountjoy, D. M. Pickup, R. Anderson, G. Wallidge, M. A. Holland, R. J. Newport, M. E. Smith, *Phys. Chem. Chem. Phys.* **2000**, *2*, 2455.
[21] G. Mountjoy, R. Anderson, R. J. Newport, M. E. Smith, *J. Phys. Condens. Matter* **2000**, *12*, 3505.
[22] D. M. Pickup, G. Mountjoy, M. A. Holland, G. Wallidge, R. J. Newport, M. E. Smith, *J. Mater. Chem.* **2000**, *10*, 1887.
[23] G. Mountjoy, D. M. Pickup, G. Wallidge, R. Anderson, J. M. Cole, M. E. Smith, R. J. Newport, *Chem. Mater.* **1999**, *11*, 1253.
[24] D. M. Pickup, G. Mountjoy, M. A. Holland, G. Wallidge, R. J. Newport, M. E. Smith, *J. Phys. Condens. Matter* **2000**, *12*, 9751.
[25] R. Anderson, G. Mountjoy, M. E. Smith, R. J. Newport, *J. Non-Cryst. Solids* **1998**, *234*, 72.
[26] G. Mountjoy, M. A. Holland, G. Wallidge, P. Gunawidjaja, M. E. Smith, D. M. Pickup, R. J. Newport, *J. Phys. Chem. B* **2003**, *107*, 7557.
[27] G. Mountjoy, M. A. Holland, P. Gunawidjaja, D. M. Pickup, G. Wallidge, M. E. Smith, R. J. Newport, *J. Sol-Gel Sci. Technol.* **2003**, *26*, 137.
[28] W. Rupp, N. Hüsing, U. Schubert, *J. Mater. Chem.* **2002**, *12*, 2954.
[29] M. Puchberger, W. Rupp, U. Bauer, U. Schubert, *New J. Chem.* **2004**, *28*, 1289.
[30] V. Torma, H. Peterlik, U. Bauer, W. Rupp, N. Hüsing, S. Bernstoff, M. Steinhart, G. Goerigk, U. Schubert, *Chem. Mater.* **2005**, *17*, 3146.
[31] P. Gunawidjaja, M. A. Holland, G. Mountjoy, D. M. Pickup, R. J. Newport, M. E. Smith, *Solid State Nucl. Magn. Reson.* **2003**, *23*, 88.
[32] Y. Mao, T. J. Park, S. S. Wong, *Chem. Commun.* **2005**, 5721.
[33] L. Armelao, D. Bleiner, V. Di Noto, S. Gross, C. Sada, U. Schubert, E. Tondello, H. Vonmont, A. Zattin, *Appl. Surf. Sci.* **2005**, *249*, 277.
[34] L. Armelao, C. Eisenmenger-Sittner, M. Groenewolt, S. Gross, C. Sada, U. Schubert, E. Tondello, A. Zattin, *J. Mater. Chem.* **2005**, *15*, 1838.
[35] L. Armelao, H. Bertagnolli, S. Gross, V. Krishnan, U. Lavrencic-Stangar, K. Müller, B. Orel, G. Srinivasan, E. Tondello, A. Zattin, *J. Mater. Chem.* **2005**, *15*, 1954.
[36] L. Armelao, S. Gross, E. Tondello, A. Zattin, *Surf. Sci. Spectra* **2005**, *10*, 157.
[37] L. Armelao, S. Gross, E. Tondello, A. Zattin, *Surf. Sci. Spectra* **2005**, *10*, 150.
[38] L. Armelao, D. Barreca, G. Bottaro, A. Gasparotto, S. Gross, C. Maragno, E. Tondello, A. Zattin, *Surf. Sci. Spectra* **2005**, *10*, 137.
[39] G. Trimmel, S. Gross, G. Kickelbick, U. Schubert, *Appl. Organomet. Chem.* **2001**, *15*, 410.
[40] S. Gross, G. Kickelbick, M. Puchberger, U. Schubert, *Monatsh. Chem.* **2003**, *134*, 1053.
[41] U. Schubert, *Chem. Mater.* **2001**, *13*, 3487.
[42] G. Kickelbick, *Prog. Polym. Sci.* **2003**, *28*, 83.

[43] U. Schubert, *J. Sol–Gel Sci. Technol.* **2003**, *26*, 47.
[44] U. Schubert, in *Organic/Inorganic Hybrid Materials*, Electronic Publ. Services, Hattiesburg **2003**.
[45] F. Del Monte, W. Larsen, J. D. Mackenzie, *J. Am. Ceram. Soc.* **2000**, *83*, 628.
[46] T. Nishide, S. Honda, M. Matsuura, M. Ide, *Thin Solid Films* **2000**, *371*, 61.
[47] P. Innocenzi, *J. Non-Cryst. Solids* **2003**, *319*, 309.
[48] D. M. Pickup, G. Mountjoy, G. W. Wallidge, R. J. Newoprt, M. E. Smith, *Phys. Chem. Chem. Phys.* **1999**, *1*, 2527.
[49] A. Bertoluzza, C. Fagnano, M. A. Morelli, V. Gottardi, M. Guglielmi, *J. Non-Cryst. Solids* **1982**, *48*, 117.
[50] C. M. Parler, J. A. Ritter, M. D. Amiridis, *J. Non-Cryst. Solids* **2001**, *279*, 119.
[51] F. Moulder, W. F. Stickle, P. E. Sobol, K. D. Bomben, in *Handbook of X-Ray Photoelectron Spectroscopy*, Perkin-Elmer, Eden Prairie, MN **1991**.
[52] S. C. Moon, M. Fujino, V. H. Yamashita, M. Anpo, *J. Phys. Chem. B* **1997**, *101*, 369.
[53] R. K. Iler, in *The Chemistry of Silica*, Wiley, New York **1979**.
[54] M. I. Osendi, J. S. Moya, C. J. Serna, J. Soria, *J. Am. Ceram. Soc.* **1985**, *68*, 135.
[55] R. C. Garvie, *J. Phys. Chem.* **1965**, *69*, 1238.
[56] R. C. Garvie, *J. Phys. Chem.* **1978**, *82*, 218.
[57] V. S. Nagarajan, K. J. Rao, *J. Mater. Sci.* **1989**, *24*, 2140.
[58] F. F. Lange, *J. Mater. Sci.* **1982**, *17*, 225.
[59] F. F. Lange, *J. Mater. Sci.* **1982**, *17*, 235.
[60] H. Heuer, N. Claussen, W. M. Kriven, M. Rühle, *J. Am. Ceram. Soc.* **1982**, *65*, 642.
[61] G. Skandan, H. Hahn, M. Roddy, W. R. Cannon, *J. Am. Ceram. Soc.* **1994**, *77*, 1706.
[62] K. V. Terry, C. G. Lugmair, T. D. Tilley, *J. Am. Chem. Soc.* **1997**, *119*, 9745.
[63] H. J. M. Bosman, E. C. Kruissink, J. Vanderspoel, F. Vanderbrink, *J. Catal.* **1994**, *148*, 660.
[64] L. Armelao, R. Bertoncello, S. Coronaro, A. Glisenti, *Sci. Technol. Cult. Heritage* **1998**, *7*, 4.
[65] D. Briggs, M. P. Seah, in *Practical Surface Analysis*, Wiley, New York **1990**.
[66] T. S. Ertel, H. Bertagnolli, S. Hückmann, U. Kolb, D. Peter, *Appl. Spectrosc.* **1992**, *46*, 690.
[67] M. Newville, P. Livins, Y. Yakoby, J. J. Rehr, E. A. Stern, *Phys. Rev. B: Condens. Matter Mater. Phys.* **1993**, *47*, 14 126.
[68] S. J. Gurman, N. Binstead, I. Ross, *J. Phys. C: Solid State Phys.* **1986**, *19*, 1845.